Experimental validation of model for pulsed-laser-induced subsurface modifications in Si

P.C. Verburg[*1], G.R.B.E. Römer[*1], G.H.M. Knippels[*2], J. Betz[*2], A.J. Huis in 't Veld[*1,3]

[*1] *University of Twente, Faculty of Engineering Technology, Chair of Applied Laser Technology, P.O. box 217, 7500 AE Enschede, The Netherlands.*
[*2] *Advanced Laser Separation International (ALSI) N.V., Platinawerf 20-G, 6641 TL Beuningen (Gld), The Netherlands.*
[*3] *TNO Technical Sciences; Mechatronics, Mechanics and Materials, De Rondom 1, 5600 HE Eindhoven, The Netherlands.*

Wafers are traditionally diced with diamond saw blades. Saw dicing technology has a number of limitations, especially concerning the dicing of thin wafers. Moreover, the use of fluids and the generation of debris can damage fragile components such as micro electro-mechanical systems. Laser ablation dicing is better suited for thin wafers, but is also not a clean process. An alternative dicing method is subsurface laser dicing. This technology is based on the production of laser-induced subsurface modifications inside the wafer. These modifications weaken the material, such that the wafer separates along the planes with laser modifications when applying an external force. To find the right laser conditions to produce subsurface modifications in silicon, and to enhance the understanding of the underlying physics, a numerical model has previously been developed. To validate this model, the current work compares simulation results with experimental data obtained by focusing nano- and picosecond pulses inside silicon wafers. A fairly good agreement between experimental and numerical results was obtained.

Keywords: Laser, wafer, dicing, subsurface, silicon, two-temperature model.

1. Introduction

Wafer dicing is the process to cut wafers into separate dies. Traditionally, wafers are cut by diamond saw blades [1]. New developments in the semiconductor industry such as micro electro-mechanical systems (MEMS) and die stacking pose significant challenges to the wafer dicing process [2]. Damage to the dies as a result of debris or the use of cleaning and cooling fluids, are the most important issues when dicing MEMS. For die stacking, the required thin dies are challenging to dice.

Several alternative dicing methods have been proposed. Examples are laser ablation dicing [3], laser microjet separation [4] and thermal laser separation [5]. Laser ablation dicing is more suitable for thin and brittle materials than saw dicing [2]. However, it is not a clean process. The current research is focused on laser-induced subsurface separation [6]. Together with thermal laser separation with dry cooling [7], this technology is the most promising for dicing of MEMS as it is a clean and dry process.

Subsurface laser dicing uses a laser beam that is sharply focused inside the wafer. The wavelength should be selected such that the photon energy is around or below the band-gap of the semiconductor, to ensure that the material is mostly transparent to the laser beam. By employing multi-photon absorption or the temperature dependence of the linear absorption coefficient, selective absorption of the laser energy inside the wafer can be triggered. The localized absorption of laser light leads to a modification of the material. These modifications (see Figure 1) locally weaken the wafer. In a second step, the wafer separates along the planes with laser-induced modifications, when an external force is applied (see Figure 2). This force can be applied by expanding the dicing tape the wafer is attached to.

The generation of laser-induced subsurface modifications in silicon has previously been investigated by a numerical model [8]. The purpose of the present work is to validate these numerical results.

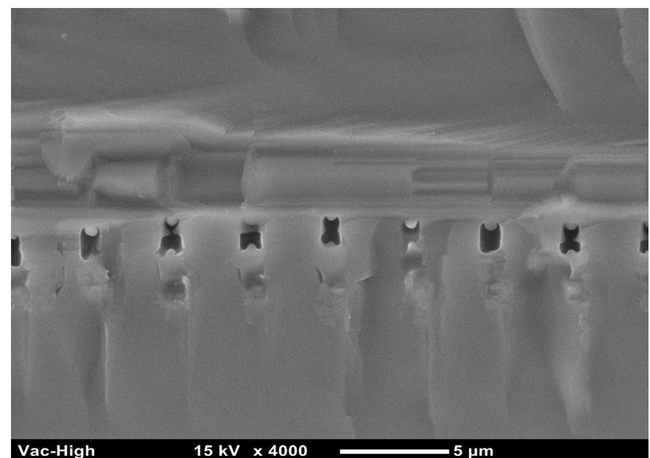

Figure 1: Scanning electron microscopy image of the sidewalls of the die after dicing. Wavelength: 1064 nm, full width at half maximum (FWHM) pulse duration: 47 ns.

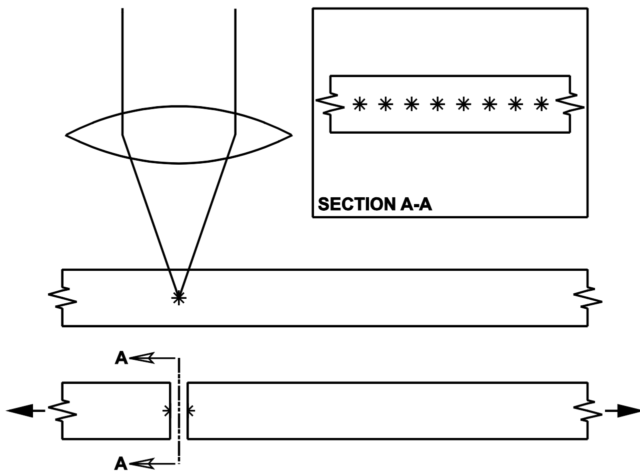

Figure 2: The production of subsurface modifications (*) and subsequent dicing by applying an external force.

2. Numerical simulations

Previously, numerical simulations have been performed to simulate the production of subsurface modifications in silicon [8]. These simulations consist of four distributions that are solved as a function of time, using the finite element method: (1) the lattice temperature, (2) the electron temperature, (3) the density of free carriers and (4) the laser light intensity. During those simulations the following physical phenomena were taken into account: (1) single-photon absorption, (2) two-photon absorption, (3) free carrier absorption, (4) the generation and recombination of electron-hole pairs, (5) diffusion of heat and free carriers, (6) the electron-phonon coupling and (7) latent heat.

In the simulations a modification was defined as the volume that reached the liquid phase, assuming that after fast resolidification a change to the material structure has occurred. An example of a simulated modification shape is shown in Figure 3; the horizontal axis coincides with the optical axis of the laser beam.

It was shown that, for a photon energy near the band-gap of silicon, nanosecond pulses are required to successfully produce subsurface modifications in silicon. This is demonstrated in Figure 4, by plotting the subsurface modification length along the optical axis as a function of the pulse duration and pulse energy.

For the near band-gap photon energy, the temperature dependence of the interband absorption coefficient is critical to produce subsurface modifications. The selected wavelength should result in a low, but not negligible, linear absorption coefficient at room temperature. This ensures that the laser energy is not absorbed before reaching the focus location. As the laser energy absorption is more concentrated near the focus, the increase in temperature and carrier density will be higher than in the surrounding material. Since the linear absorption coefficient quickly rises with temperature, a thermal runaway is triggered.

According to the simulations, picosecond pulses with a similar wavelength result in too much two-photon absorption outside the focus of the laser beam, when employing a focusing objective with a numerical aperture of 0.7. The resulting electron-hole plasma further shields the laser beam from reaching the focus, due to strong free carrier absorption.

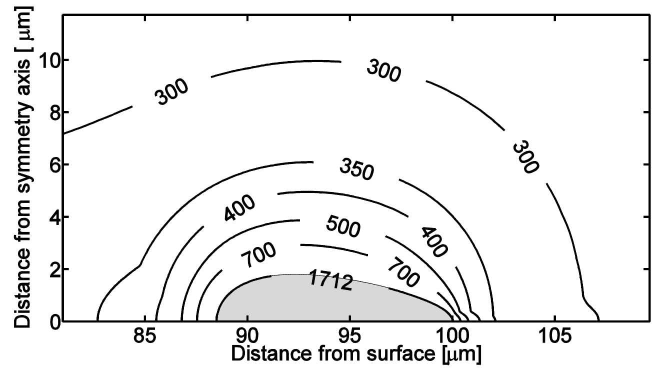

Figure 3: Contour plot of maximum lattice temperatures [K]. The gray area has reached the liquid phase. Wavelength: 1064 nm, focus depth: 100 µm, numerical aperture: 0.7, pulse energy: 2 µJ, FWHM pulse duration: 50 ns, M^2: 1.3.

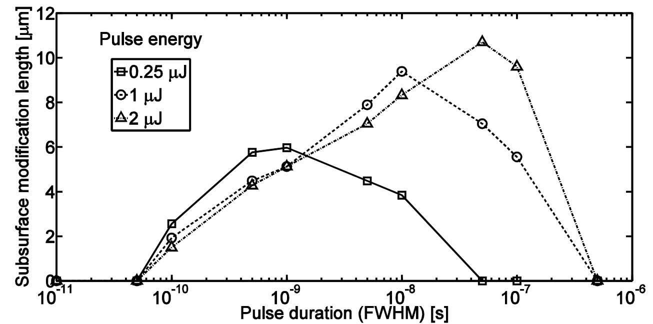

Figure 4: Subsurface modification length as a function of pulse duration and pulse energy. Wavelength: 1064 nm, focus depth: 100 µm, numerical aperture: 0.7, M^2: 1.3.

3. Experimental setups

3.1. Laser sources

To validate the numerical results shown in the previous section, three different lasers were used. Their full width at half maximum (FWHM) pulse durations range from 6.6 ps to 170 ns. All laser sources provide a photon energy that is close to the band-gap of silicon. The picosecond laser is a Trumpf Trumicro 5050. A Spectra Physics Quanta Ray GCR-270 was used to produce 8 ns pulses and a SPI SP-20P-SM-B-B-A-B was employed to generate 170 ns pulses. The specifications of these sources can be found in Table 1, Table 2 and Table 3 respectively.

Laser type	Yb:YAG disk laser
Pulse duration (FWHM)	6.6 ps
Peak wavelength	1030 nm
Maximum pulse energy	125 µJ
Maximum Repetition rate	400 kHz

Table 1: Properties of the Trumpf Trumicro 5050 source.

Laser type	Nd:YAG rod laser
Pulse duration (FWHM)	8 ns
Peak wavelength	1064 nm
Maximum pulse energy	1750 mJ
Maximum repetition rate	15 Hz

Table 2: Properties of the Spectra Physics Quanta Ray GCR-270 source.

Laser type	Fiber laser
Pulse duration (FWHM)	170 ns (tunable)
Peak wavelength	1062 +/- 3 nm
Maximum pulse energy	550 µJ
Maximum Repetition rate	1 mHz

Table 3: Properties of the SPI SP-20P-SM-B-B-A-B source.

There is a small difference in peak wavelength between the picosecond and nanosecond sources. Since the inter-band absorption coefficient of silicon shows a high gradient near the band-gap, this will affect the results. To assess the influence of this difference, the simulations described in [8] have been repeated with a wavelength of 1030 nm. A comparison between both wavelengths is shown in Figure 5 for a pulse energy of 2 µJ. According to the simulations, the 1030 nm wavelength offers a slightly inferior compromise between achieving absorption in the focal zone and preventing excessive losses elsewhere in the beam path. Despite of this observation, the general dependence of the modification length on the pulse duration remains similar.

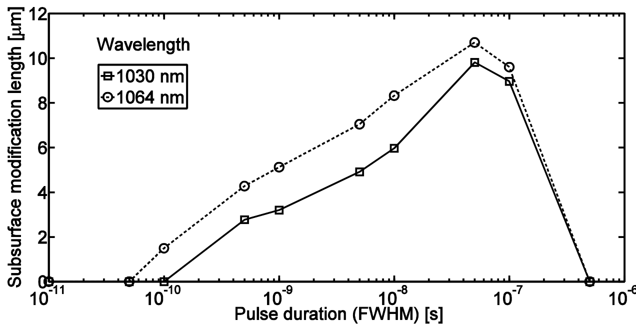

Figure 5: Subsurface modification length as a function of pulse duration and wavelength. Focus depth: 100 µm, numerical aperture: 0.7, pulse energy: 2 µJ, M^2: 1.3.

3.2. Prototype setup

The experimental setup that was used for the current research is intended to focus the laser beam to a close to diffraction limited spot inside silicon samples. The focusing objective is a Leica 11 101 666 infrared microscope objective that has a fixed cover correction for 100 µm of silicon. The numerical aperture of the objective is 0.7. A schematic overview of the experimental setup is shown in Figure 6. The silicon samples were mounted on a carbon membrane with better than 500 nm flatness, attached to a vacuum chamber. This vacuum chamber is connected to a crossed roller bearing stage with 5 degrees of freedom, to position the sample with respect to the objective. The translation along the optical axis was set by a differential micrometer. A Sill Optics S6ASS5310 beam expander was used to adapt the laser beam diameter.

To establish a reference positions for the focus location, a low power beam was focused at the surface of the silicon sample. The focus was determined by observing the reflection of the laser spot with a CMOS camera. A small percentage of the light reflected by the sample is transmitted through the dielectric mirror that steers the incoming laser beam towards the focusing objective. Since this mirror is polished on both sides, the transmitted light can be used for measurements. The imaging lens in front of the CMOS camera was aligned by removing the objective and focusing the reflected laser beam. The correctness of the focus measurement was tested by shifting the sample in micrometer steps along the optical axis, around the focus position indicated by the camera. At each position a low energy pulse was released, that is just capable of melting the surface at the peak fluence.

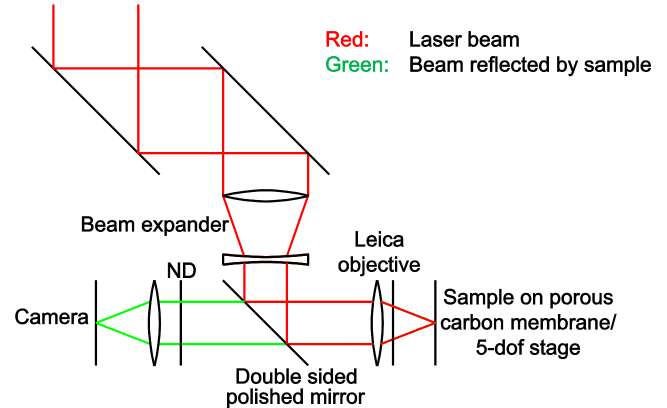

Figure 6: Schematic drawing of the experimental setup.

3.3. Laser dicing machine

In addition to the prototype setup that was discussed in the previous section, a laser dicing machine was employed. This machine is connected to the SPI fiber laser. The laser beam is focused by a Leica 11 101 887 objective. This objective contains the same optical elements as the objective used in the prototype setup, but has a variable instead of a fixed cover correction. In the laser dicing machine the objective is set to the maximum cover correction. By varying the thickness of the cover glass, the effective cover correction can be adapted to the focus depth inside the wafer. This configuration uses a fixed beam diameter such that 99% of the laser energy falls within the back aperture of the objective.

3.4. Analysis methods

For detailed observations of the structure of the subsurface modifications, destructive methods are required. To detect the presence of modifications in a non-destructive manner, infrared transmission microscopy was used. The infrared microscope is a Leica DMRM equipped with a halogen bulb and long pass filter below the stage and a CMOS camera without an infrared filter. An example of an infrared image of subsurface modifications in silicon is shown in Figure 7.

The sidewalls of the dies were inspected by a Leica DMRM optical microscope, a Keyence VK-9710 laser scanning confocal microscope and a Jeol JCM-5000 scanning electron microscope. When analyzing fractured surfaces, a single picture may not reveal the complete laser modification due to variations in the fracture plane.

4. Experimental results

4.1. Sample material

For the experimental research 160 µm thick silicon samples with a resistivity of 10.3 Ωcm were machined. To allow for better inspection of the interior of the wafers by infrared transmission microscopy, the wafers are double sided polished.

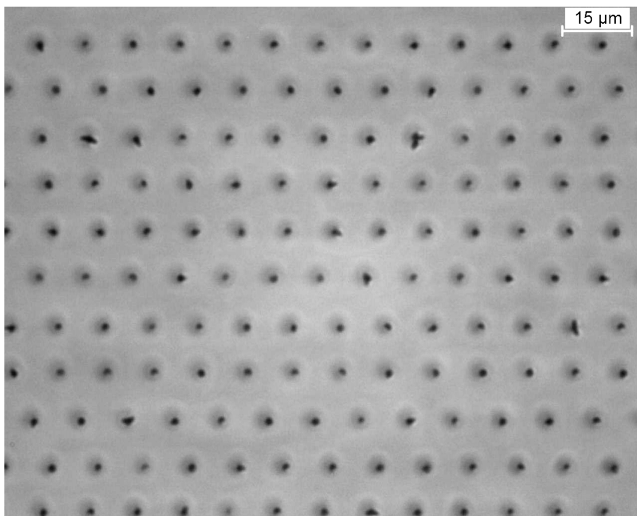

Figure 7: Infrared transmission microscopy image of laser-induced subsurface modifications in silicon. Wavelength: 1064 nm, FWHM pulse duration: 47 ns.

4.2. Picosecond pulses

A range of pulse energies from 25 nJ to 2.5 µJ was investigated. The focus depth was set to 100 µm below the silicon surface. Different $1/e^2$ beam diameters between 2 and 5 mm were tested. The smallest beam diameter gives an almost non-truncated Gaussian beam, for the 5 mm beam the $1/e^2$ diameter fills the back aperture of the objective. No subsurface modifications were observed by infrared transmission microscopy. At a pulse energy of approximately 0.3 µJ and 1.75 µJ for the 2 and 5 mm beams respectively, a surface modification starts to appear.

4.3. Nanosecond pulses

Both nanosecond laser sources were found to be suitable for the production of subsurface modifications in silicon. Therefore, in addition to the prototype setup, the laser dicing machine was used to accurately position modifications along planes inside the sample. This allows for the samples to be diced. After dicing a comparison was made between the pulse energy and the modification length along the optical axis.

A range of pulse energies from 0.5 to 14 µJ was analyzed. The laser pulses were positioned at a depth of 130 µm inside the 160 µm thick wafers. An additional layer of modifications was placed near the front surface, to increase the chance of successfully dicing the samples. The modifications were spaced 10 µm apart. This is a compromise between allowing for individual modifications to be analyzed and the ability to dice the samples along the planes defined by the laser modifications.

At pulse energies between 2 and 5 µJ, modifications were observed that start at the focus position and extend towards the incoming laser beam (see Figure 8). At 1 µJ and below no modifications could be detected by infrared transmission microscopy. Above a pulse energy of 5.2 µJ, many modifications were showing an irregular profile (see Figure 9). Further investigation is required to determine the cause of these shapes. Both the intensity profile at large distances from the focus and variations in the fracture plane may be influencing factors.

Figure 8: Laser scanning confocal microscopy intensity image of the sidewalls of the die after dicing, laser beam propagation direction: top-down. Wavelength: 1062nm, FWHM pulse duration: 170 ns, pulse energy: 5.2 µJ, focus depth: 130 µm, M^2: 1.1.

Figure 9: Laser scanning confocal microscopy intensity image of the sidewalls of the die after dicing, laser beam propagation direction: top-down. Wavelength: 1062nm, FWHM pulse duration: 170 ns, pulse energy: 9.35 µJ, focus depth: 130 µm, M^2: 1.1.

4.4. Validation of the numerical model

The simulation results shown in Figure 3, predict that picosecond pulses with a photon energy near the band-gap of silicon do not result in subsurface modifications, when using the optical system available in the experimental setup. The experiments with the Trumpf Trumicro picosecond laser source confirm this prediction. Both nanosecond lasers were successfully used to generate subsurface modifications. Their pulse durations (8 and 170 ns) indeed fall within the range predicted by the model.

Additionally, to allow for a quantitative verification of the model results, the length along the optical axis of the subsurface modifications was compared with the predictions from the model, for pulse energies up to 5.2 µJ. This range of pulse energies resulted in modifications that are continuous along the optical axis. The 170 ns pulses were simulated by a constant intensity during the pulse duration. The results of this comparison are shown in Figure 10. A fairly good agreement between the numerical predictions and experimental results is observed.

Due to the limited dataset, an estimate of the uncertainty in the experimental measurements is not yet available. Especially variations in the breaking plane are a source of inaccuracies.

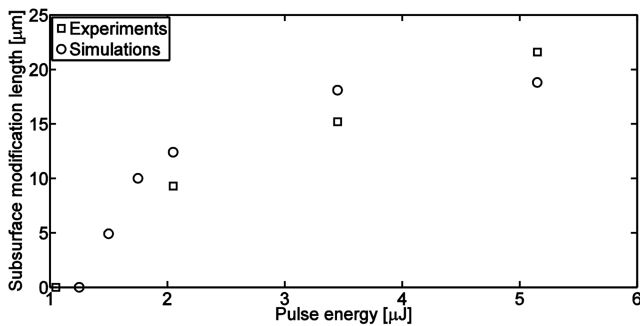

Figure 10: Simulated and experimental modification lengths as a function of pulse energy. Wavelength: 1062 nm, FWHM pulse duration: 170 ns, focus depth: 130 µm, M^2: 1.1.

5. Discussion

Overall, a fairly good match between numerical simulations and experimental data was observed, both in terms of the size of the modifications as a function of pulse energy and in terms of the dependence on the pulse duration. At high pulse energies, irregular-shaped modifications were found that need further investigation. Additionally, more experimental data is required to assess the accuracy of the measurements.

The focus depth inside the wafers was fixed during this study; future work will include the dependence of the properties of modifications on the focus depth. All lasers used for the current work provide a photon energy close to the band-gap of silicon. A photon energy significantly below the band-gap may also be investigated. Multi-photon absorption is then required to selectively absorb the laser energy in the bulk of the wafer.

Finally, the exact material phases that are created as a result of the melting and rapid resolidification need to be analyzed. Preliminary results have shown that selected area diffraction is a suitable technology for this purpose.

6. Conclusions

Subsurface modifications were produced by focusing laser pulses inside silicon wafers. The experimental results were compared with numerical simulations including heat transfer, carrier dynamics and several mechanisms of laser energy absorption. The required laser parameters to produce subsurface modifications were correctly predicted by the model. Up to a pulse energy of 5.2 µJ, quantitative predictions of the modification size were possible. Future work is required to increase the accuracy of the experimental results, study the influence of additional laser parameters on the properties of the subsurface modifications and to obtain detailed information about the material phases.

References

[1] H. Tönshoff, W. v. Schmieden, I. Inasaki, W. König, and G. Spur, "Abrasive machining of silicon," *CIRP Annals - Manufacturing Technology*, vol. 39, no. 2, pp. 621–635, 1990.

[2] J. van Borkulo, R. Evertsen, and R. Hendriks, "Enabling technology in thin wafer dicing," *ECS Transactions*, vol. 18, pp. 837–842, 2009.

[3] A. Yokotani, N. Matsuo, K. Kawahara, Y. Kurogi, N. Matsuo, T. Ninomiya, H. Sawada, and K. Kurosawa, "Development of dicing technique for thin semiconductor substrates with femtosecond laser ablation," vol. 4637, pp. 180–187, SPIE, 2002.

[4] D. Perrottet, S. Green, and B. Richerzhagen, "Clean dicing of compound semiconductors using the water-jet guided laser technology," in *2006 IEEE/SEMI Advanced Semiconductor Manufacturing Conference*, pp. 233–236, 2006.

[5] O. Haupt, F. Siegel, A. Schoonderbeek, L. Richter, R. Kling, and A. Ostendorf, "Laser dicing of silicon: Comparison of ablation mechanisms with a novel technology of thermally induced stress," *Journal of Laser Micro/Nanoengineering*, vol. 3, pp. 135–140, 2008.

[6] E. Ohmura, F. Fukuyo, F. Fukumitsu, and H. Morita, "Internal modified-layer formation mechanism into silicon with nanosecond laser," *Journal of Achievements in Materials and Manufacturing Engineering*, vol. 17, pp. 381–384, 2006.

[7] H.-U. Zühlke, G. Eberhardt, and R. Ullmann, "TLS-Dicing - an innovative alternative to known technologies," in *SEMI/IEEE Advanced Semiconductor Manufacturing Conference 2009*, pp. 28–32, 2009.

[8] P. Verburg, G. Römer, and A. Huis in 't Veld, "Two-temperature model for pulsed-laser-induced subsurface modifications in Si," *To be published.*